ZnO Nanocrystals by a Non-Hydrolytic Route: Synthesis and Characterization.

ARTICLE *in* CHEMINFORM · APRIL 2003

Impact Factor: 0.74 · DOI: 10.1021/jp027533+

3 AUTHORS:

Davide Cozzoli
Università del Salento
136 PUBLICATIONS **5,721** CITATIONS
SEE PROFILE

M. L. Curri
Italian National Research Council
245 PUBLICATIONS **3,354** CITATIONS
SEE PROFILE

Angela Agostiano
Università degli Studi di Bari Aldo Moro
358 PUBLICATIONS **4,074** CITATIONS
SEE PROFILE

ZnO Nanocrystals by a Non-hydrolytic Route: Synthesis and Characterization

P. Davide Cozzoli,[†] M. Lucia Curri,[‡] and Angela Agostiano*[,†,‡]

Dipartimento di Chimica, Universita' di Bari, Via Orabona 4, 70126 Bari, Italy, and CNR-Istituto per i Processi Chimico Fisici (IPCF), sez. Bari, Via Orabona 4, 70126 Bari, Italy

Gabriella Leo[§,||] and Mauro Lomascolo[§]

Istituto di Microelettronica e Microsistemi (IMM)-CNR, Sez. Lecce, Via Arnesano, 73100 Lecce, Italy, and Istituto per lo Studio dei Materiali Nanostrutturati (ISMN) CNR, Area della Ricerca di Roma, Via Salaria Km 29.3, 00016 Monterotondo, Roma, Italy

Received: November 22, 2002; In Final Form: February 26, 2003

We report a novel, non-hydrolytic route to ZnO nanocrystals by means of thermal decomposition of zinc acetate ($ZnAc_2$) in alkylamines, in the presence of *tert*-butylphosphonic acid (TBPA). The slow heating of an alkylamine/TBPA/$ZnAc_2$ mixture is a simple, safe, and scalable approach to synthesize ZnO nanocrystals from handy chemicals. The obtained ZnO nanocrystals were characterized by UV−vis absorption, photoluminescence (PL) and infrared (FT-IR) spectroscopies, and by X-ray diffraction (XRD) and transmission electron microscopy (TEM). The growth of ZnO particles in the nanoscopic regime and their final size were governed by the TBPA/$ZnAc_2$ molar ratio in the reaction mixtures. The various roles played by TBPA in the conditions of the synthesis are discussed on the basis of the experimental evidence. The presented synthetic approach provides a unique tool for designing the synthesis of ZnO crystals of a desired size in the nanoscale regime and can be potentially extended to other nanoscale materials.

1. Introduction

Research on zinc oxide nanocrystals[1] has increased enormously during the past years due to their envisaged applications in many technologies, such as solar energy conversion,[2,3] optoelectronic devices,[4,5] and catalysis.[6]

Recently, there have been several reports of solution-phase synthesis of ZnO colloids at low temperature, mainly based on the hydrolysis of zinc salts[1,7−9] or zinc alkoxides[10,11] in organic solvents, and on electrochemical routes.[12,13] In addition, polymers[14,15] and reverse micelles[11,16] have been exploited in order to control both particle morphologies and sizes. However, unless extreme thermal treatments are applied after the synthesis, such preparative routes provide nanocrystalline ZnO with hydroxylated surfaces, with adsorbed water, and organic molecules, that can significantly affect material properties. Surface-related defects account for both radiative and nonradiative decay channels competing with the ZnO band-edge emission,[17] while surface-bound molecules[18,19] or acid−basic sites can influence emission properties as well as redox potentials and interfacial electron-transfer rates.[20] In this scenario, the development of synthetic non-hydrolytic approaches and the use of coordination chemistry could provide some control over the surface of nanocrystals by passivation of surface traps and/or by ready exchange of surface-capping ligands.

Developments in the synthesis of II−VI semiconductor nanoparticles have recently demonstrated the potential of the thermal decomposition of organometallic precursors in coordinating solvents[21] to prepare high-quality metal oxide nanocrystals.[22,23] A high-temperature synthesis of TOPO- and amine-capped ZnO nanocrystals, using diethylzinc as metal precursor, has also been reported.[24] However, the use of less toxic and more easily handy precursors would be of valuable technological interest to allow a scale-up of nanocrystal synthesis.

In this paper, we describe an alternative preparation of organic-capped ZnO nanocrystals by the thermal decomposition of zinc acetate ($ZnAc_2$) in a high-temperature coordinating mixture of a long-chain alkylamine and *tert*-butylphosphonic acid (TBPA). The ZnO particles were characterized by UV−vis absorption, infrared (IR) and photoluminescence (PL) spectroscopy, powder X-ray diffraction (XRD), and transmission electron microscopy (TEM). The variation of the TBPA/$ZnAc_2$ molar ratio allowed the tuning of the nanocrystal size in the range 3−9 nm. The addition of the phosphonic acid is discussed in relation to its effectiveness in directing ZnO crystal growth in the quantum confinement regime. The role of the surface in the emission properties of the nanoparticles and the stability of amine/TBPA-coated ZnO nanocrystals are also outlined.

2. Experimental Section

2.1. Materials. Anhydrous zinc acetate ($Zn(CH_3CO_2)_2$ or $ZnAc_2$, 99.99%), *n*-octylamine ($C_8H_{17}NH_2$ or OA, 99%), tri-*n*-octylamine $(C_8H_{17})_3N$ or TOA, 98%), tri-*n*-octyphosphine oxide ($(C_8H_{17})_3PO$ or TOPO, 99%), *n*-hexadecylamine ($C_{16}H_{33}NH_2$ or HDA, 90%), and *n*-dodecylamine ($C_{12}H_{25}NH_2$ or DDA, 98%) were purchased from Fluka. *tert*-Butylphosphonic acid ($C_4H_9PO(OH)_2$ or TBPA 98%) was purchased from Aldrich; *n*-octyl-($C_8H_{17}PO(OH)_2$ 98% or OPA), *n*-tetradecyl-($C_{14}H_{29}PO(OH)_2$ or TDPA 98%), and *n*-octadecylphosphonic ($C_{18}H_{37}PO(OH)_2$ or ODPA 98%) acids were purchased from Alfa Aesar. All chemicals were of the highest purity available and were used

* Author to whom correspondence should be addressed at CNR-IPCF c/o Dipartimento di Chimica, Via Orabona 4, 70125 Bari, Italy. E-mail: agostiano@area.ba.cnr.it.

[†] Universita' di Bari.

[‡] CNR-Istituto per i Processi Chimico Fisici (IPCF).

[§] Istituto di Microelettronica e Microsistemi (IMM)-CNR.

[||] Istituto per lo Studio dei Materiali Nanostrutturati (ISMN) CNR.

10.1021/jp027533+ CCC: $25.00
Published on Web 04/24/2003

as received without further purification or distillation. All solvents used were of analytical grade and were purchased from Aldrich.

2.2. Synthesis of ZnO Nanoparticles. *Direct Injection Method.* All manipulations were performed using standard air-free techniques, unless otherwise stated. A 0.2−0.8 M solution of $ZnAc_2$ precursor was prepared by dissolving the appropriate amount of $ZnAc_2$ in OA, then by degassing the solution under vacuum at 60 °C for 1 h, under vigorous stirring. This solution was finally cooled to room temperature and kept under nitrogen flow. In a typical synthesis, 5−10 g of a mixture of an alkylamine and TBPA (TBPA: $ZnAc_2$ molar ratio was always kept less than ∼0.70) was degassed at 120 °C for 1 h under vigorous stirring in a 25 mL three-neck flask connected to a Liebig condenser, after which it was heated to high temperatures (in the range 220−300 °C) under nitrogen flow. A volume of 2−4 mL of the $ZnAc_2$ precursor solution was loaded into a 5 mL syringe and then was rapidly injected. Upon injection of the precursor, the temperature dropped to about 180−240 °C and was maintained at these levels throughout the synthesis. The growth kinetics of the nanoparticles was monitored by taking aliquots of the reaction mixture at different times from injection. These samples were immediately cooled and diluted with chloroform to stop particle growth and to provide appropriate optical density for absorption spectra. When no further significant growth of the particles was observed, the reaction was stopped by just removing the heat source and rapidly cooling the flask.

Slow Heating Method. ZnO nanocrystals were directly grown in alkylamines by slowly heating the reaction mixture to high temperatures according to the following procedure: 0.5−2 mmol of $ZnAc_2$ was dissolved in 5−10 g of an alkylamine−TBPA mixture at 80 °C, and then degassed under vacuum for 1 h under vigorous stirring. The reaction vessel was then slowly heated under nitrogen at a rate of 10 °C/min to induce the decomposition of $ZnAc_2$; the temperature at which the first ZnO absorption features were detected was fixed as the temperature for further growth (T_{gr}). T_{gr} generally lay in the range of 220−300 °C, depending on TBPA/$ZnAc_2$ molar ratio (R). The growth kinetics of the nanoparticles was monitored as described above.

Extraction Procedures. The extraction procedures were subsequently performed in air: ZnO nanocrystals were readily precipitated upon addition of ethanol to the reaction mixture at 50 °C before solidification took place. The resulting precipitate was isolated by centrifugation and was washed twice with ethanol to remove residual surfactants. The surfactant-coated ZnO nanoparticles were then easily re-dispersed in solvents such as $CHCl_3$ or hexane, without any further growth or irreversible aggregation, and used for spectroscopic measurements and TEM investigations.

ZnO powders for XRD analysis and IR measurements were prepared by washing the extracted precipitate repeatedly and then evaporating the residual solvent under vacuum at 100 °C for 4 h.

2.3. Characterization of Samples. *UV−vis Absorption Spectroscopy.* To monitor the nanocrystal growth, absorption spectra were measured using an Ocean UV−vis diode array spectrometer equipped with an optical fiber and a deuterium lamp. Appropriate blank solutions of amine/TBPA in $CHCl_3$ were used as references. Room-temperature absorption spectra were taken using a Cary 3 (Varian) spectrophotometer.

Photoluminescence Spectroscopy. Photoluminescence (PL) spectra of isolated ZnO nanoparticles in chloroform were measured at room temperature with a FluoroMax-2 spectrofluorimeter. Appropriate filters to avoid second-order contributions were installed in the emission light path. PL spectra were measured of colloidal solutions having an optical density less than 0.3 at 280 nm to avoid reabsorption effects. PL spectra were normalized to the value of absorbance at the excitation wavelength.

Infrared Spectroscopy. FTIR spectra of ZnO powder were collected with a Bruker Equinox 55 spectrometer with a resolution of 4 cm^{-1}. Measurements were performed with pressed pellets which were made using KBr powder as diluent.

Powder X-ray Diffraction. XRD patterns of ZnO nanocrystal powders were collected with a Philips PW1729 diffractometer in a conventional $\theta-2\theta$ reflection geometry using filtered Cu Kα radiation ($\lambda = 1.54056$ Å). For XRD measurements, the nanocrystal powder was placed on an Al sample holder.

Transmission Electron Microscopy. Transmission electron microscopy (TEM) and high-resolution TEM (HRTEM) images were obtained using a Philips CM-300 microscope operating at 300 kV. The samples were prepared by dropping dilute solutions of isolated ZnO nanoparticles in chloroform onto 400-mesh carbon-coated copper grids and immediately evaporating the solvent. The samples were stable under the electron beam and did not degrade within the typical observation time.

3. Results

3.1. Synthesis of ZnO Nanoparticles in Amines/TBPA. ZnO particles were grown in *n*-hexadecylamine (HDA), *n*-dodecylamine (DDA), and tri-*n*-octylamine (TOA), by using both the slow heating method and the direct injection method described above. In all cases, the presence of *tert*-butylphosphonic acid (TBPA) could guarantee the controlled growth of ZnO crystals in the nanoscopic regime.

TOPO[24] and phosphonic acids[25] were also tested as potential stabilizers, and added to the amine solution. In the case of TOPO or long linear chain phosphonic acids (OPA, TDPA, and ODPA), at low stabilizer/amine molar ratio (<0.2), no significant differences were found with respect to the synthesis performed in pure amines: bulk ZnO immediately precipitated upon injection of the precursor solution into the hot vessel (direct injection method), or as soon as $T \sim 200$ °C was reached with the slow heating method. At higher stabilizer content, only the transient formation of very small ZnO nanoparticles was detected.

When TBPA was used as stabilizer, the growth kinetics of ZnO nanocrystals exhibited some unique characteristics. After an induction period (of a few minutes), depending on TBPA/$ZnAc_2$ molar ratio (R), the optical features of ZnO were detected, after which growth was seen to proceed rapidly (generally within 5−6 min), and it finally slowed considerably. Precipitation of ZnO nanocrystals in the reaction vessel was observed only after long reaction times (>2 h) and only at $R < 0.40$.

In Figure 1 we report the UV−vis absorption spectra recorded at different stages of the particle growth during a typical synthesis done by the slow heating method (in HDA at $R = 0.22$). Upon heating at 10 °C/min, ZnO absorption features clearly appeared as soon as a characteristic temperature T_{gr} ($T_{gr} \sim 240$ °C in this specific case) had been reached (Figure 1b).

Further growth was then allowed to continue at T_{gr}: the onset of the band gap absorption shifted[9] toward longer wavelengths during this period (Figure 1c). Growth proceeded to completion in a few minutes (Figure 1d), after which it practically stopped. An appreciable change in the absorption onset could be detected only after a long heating time, with a concomitant broadening of the exciton feature (Figure 1e). A similar trend was observed

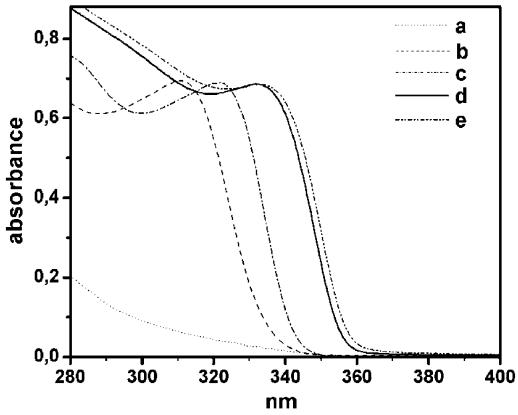

Figure 1. Temporal evolution of the absorption spectrum of ZnO particles prepared in a HDA/TBPA mixture (HDA 7 g, $ZnAc_2$ = 1 mmol, $R = 0.22$) by slowly heating the reaction mixture at 10 °C/min: (a) $ZnAc_2$ before decomposition, at 230 °C; (b) ZnO absorption features at T_{gr} = 240 °C; (c) ZnO particles grown for 3 min at T_{gr}; (d) ZnO particles grown for 5 min at T_{gr}; (e) ZnO particles grown for 120 min at T_{gr}. An appropriate blank solution of HDA/TBPA in $CHCl_3$ was used as reference.

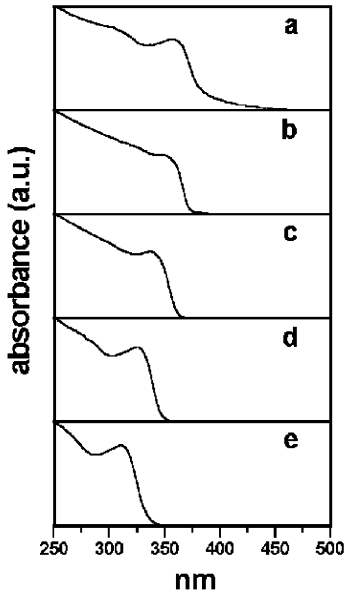

Figure 2. Size-dependent evolution of the absorption spectrum of fully grown ZnO particles as a function of TBPA/$ZnAc_2$ molar ratio, *R*, in the starting reaction mixture: (a) $R = 0$; (b) $R = 0.12$; (c) $R = 0.22$; (d) $R = 0.52$; (e) $R = 0.68$. ZnO nanocrystals were prepared by slowly heating 1 mmol of $ZnAc_2$ in 7 g of HDA, and re-dispersed in $CHCl_3$ after extraction from the reaction mixture without any size-selection. Curves have been translated vertically for the sake of clarity.

in the case of the fast injection technique. Again, an induction period (also slightly depending on the injection temperature) after the injection of the precursor solution preceded the detection of ZnO optical features. This period varied from 2 to 8 min, depending on the injection temperature. At TBPA/$ZnAc_2$ molar ratios greater than 0.70, no formation of stable ZnO particles was observed.

Figure 2 shows the size-dependent evolution of the absorption spectrum of fully grown ZnO particles at various TBPA:$ZnAc_2$ molar ratios, *R*, in the starting reaction mixture (slow heating method in HDA). A dependence[18] of the absorption onset position on the concentration of ZnO in the solutions was observed. Therefore, to make a comparison among spectra of nanocrystals having different sizes, concentrations were adjusted to ensure approximately the same absorbance at 250 nm.

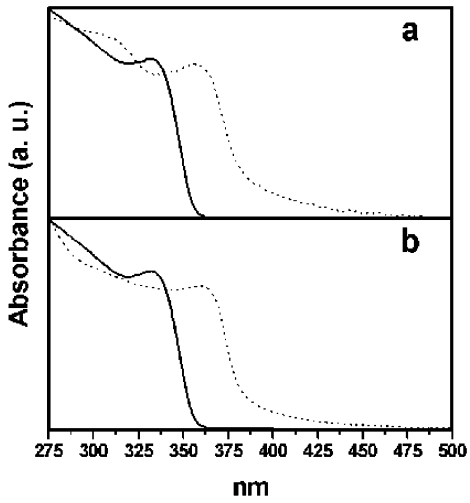

Figure 3. Absorption spectra of fully grown ZnO nanoparticles prepared by the slow heating method (a) and the direct injection method (b), without TBPA (dotted lines) and with TBPA/$ZnAc_2$ = 0.22 (solid lines). The samples were synthesized in identical growing mixtures as follows: (a) by the slow heating of 1 mmol of $ZnAc_2$ in 7 g HDA + 4 mL OA, finally fixing T_{gr} at 240 °C; (b) by the direct injection of 4 mL of a solution of $ZnAc_2$/OA 0.25 M in 7 g of HDA at 260 °C, followed by further growth at 240 °C.

In the absence of any stabilizer (Figure 2a), the onset of absorption was close to that of bulk ZnO (373 nm) and the absorption tail at wavelengths longer than 380 nm indicated that the colloidal dispersion scattered light to some extent. As all these features changed by diluting the colloidal solution, they were attributed to aggregation effects between primary clusters.[1,18] Similar behavior was shown by samples prepared in TOA and DDA and/or by the fast injection method. Moreover, a too low precursor concentration resulted only in the rapid dissolution of ZnO particles in the reaction vessel.

Samples prepared in the presence of TBPA provided optically clear organic solutions after extraction from the growing medium (see Figure 2b−e). A significant blue-shift of the band edge absorption with respect to the bulk material was measured at increasing *R*. In addition, the first exciton feature narrowed and became better resolved with decreasing particle size. The absorption spectra of ZnO nanocrystals prepared in TOA and DDA did not show any relevant difference for similar *R* values, except for a slight broadening of the exciton absorption peak.

Spectra of ZnO nanoparticles grown in HDA/TBPA mixtures by the slow heating and the fast injection methods are shown in Figure 3. No significant change in the optical features of fully grown ZnO particles prepared at the same *R*, but with different techniques, can be observed.

3.2. Infrared Spectroscopy. In Figure 4, the IR spectra in the region 2200−1300 cm^{-1} of a ZnO sample obtained by the present preparative route (in HDA at $R = 0.22$ by the slow heating method, Figure 4a) is presented; the IR spectra of pure HDA (Figure 4b) and TBPA (Figure 4c) are also reported.

The ZnO powder spectrum in Figure 4a exhibits a broad N−H bending band at about 1580 cm^{-1}, as in pure HDA; the C−H antisymmetric bending of *tert*-butyl groups in TBPA (an intense double band[27] centered at 1470 cm^{-1}), overlapping that of the methylene groups of HDA; the C−H symmetric bending of *tert*-butyl groups (a double band[27] peaking at 1390 and 1360 cm^{-1}, as in pure TBPA) overlapping that of methyl groups of HDA; the C−H and C−N bending (weak bands at 1330 and at 1316 cm^{-1} in spectrum (b) of HDA, respectively) were not observable.

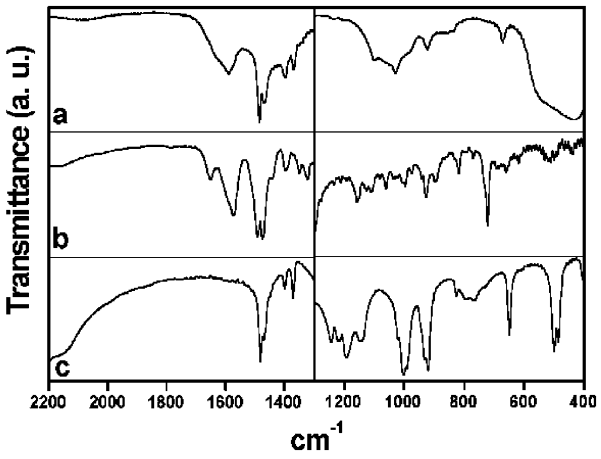

Figure 4. FT-IR spectra in the 2200−400 cm^{-1} region of (a) ZnO powder prepared in HDA at $R = 0.22$ (slow heating method); (b) HDA; (c) TBPA. The fingerprint region (below 1300 cm^{-1}) has been re-scaled for sake of clarity.

Notably, the N−H bending in the spectrum (a) results considerably broadened and slightly shifted to longer wavenumbers with respect to the position in the spectrum (b) of the pure HDA, suggesting some interaction of the aminic group with the oxide surface. The C═O and C−O stretching vibrations (two characteristic bands centered at 1580 and 1390 cm^{-1}, respectively) of acetate groups complexed with zinc[18] typically dominate in spectra of hydrolytically prepared nano-ZnO. In our sample, the presence of such bands could not be completely excluded, because of overlapping of many signals in the 1800−1300 cm^{-1} region.

In the fingerprint region (below 1400 cm^{-1}), the broadness and the complexity of the peaks make their unique interpretation quite difficult. The broad P═O stretching centered at 1200 cm^{-1} in TBPA (c) is not present in the spectrum of our ZnO sample (a), and a residual P−OH stretching band is observable at 925 cm^{-1}, together with a narrow band at 670 cm^{-1}. In addition, the narrow band at 1000 cm^{-1} in TBPA is broadened and shifted to about 1050 cm^{-1} in spectrum (a). Below 600 cm^{-1}, the characteristic stretching of Zn−O bonds in zinc oxide is observable in spectrum (a).

The disappearance of the P═O stretching and the reduction of the P−OH stretching band have already reported for ZrO_2 and TiO_2 surfaces[28] modified with phosphonic acids and interpreted as evidence for mainly tridentate and bidentate bonding modes to metal atoms on the oxide surface.

3.3. Structural and Morphological Characterization. In Figure 5, X-ray diffraction patterns, relative to samples of ZnO powder prepared in HDA/TBPA at different values of TBPA/$ZnAc_2$ molar ratio, are reported.

By comparing the diffraction peak positions with those reported in the International Crystallographic data table (ICDD), a wurtzite structure was assigned to all the samples. The figure clearly shows an increased broadening in the ZnO diffraction peaks with increasing TPBA/$ZnAc_2$ molar ratio, which correlates well with a decrease in the average nanocrystal size.

The average size, D, was estimated by using the Scherrer formula. The average nanocrystal size, D, as obtained from the full width at half-maximum (fwhm) of the (110) and (002) diffraction peaks are reported in Table 1, as a function of the TBPA/$ZnAc_2$ molar ratio.

Different sizes were obtained for the ZnO nanocrystal along the different crystallographic directions of the wurtzite structure. This position-dependent line width of the XRD patterns points to the formation of slightly elongated ZnO nanocrystals rather than spherical particles. In particular, nanocrystal sizes are larger along the (110) planes, parallel to the c-axis of the wurtzite structure, than along the (002) planes.

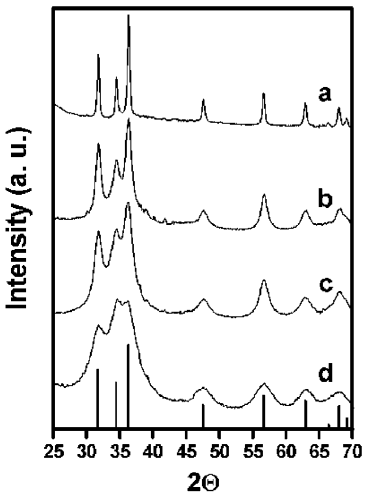

Figure 5. X-ray diffraction patterns of ZnO nanoparticle powders along with the wurtzite ZnO diffraction lines. Samples were prepared in HDA (HDA 7 g, $ZnAc_2$ 1 mmol, by the slow heating method) at different TBPA/$ZnAc_2$ molar ratios, R: (a) $R = 0$; (b) $R = 0.12$; (c) $R = 0.22$; (d) $R = 0.52$.

TABLE 1: Values of the Average ZnO Nanocrystal Size (D) Calculated by Using Scherrer's Formula for the (002) and (110) XRD Peaks as a Function of the TBPA/$ZnAc_2$ Molar Ratio, R

R	$D_{(110)}$ (nm)	$D_{(002)}$ (nm)
0.52	3.50	3.57
0.22	5.83	3.60
0.15	6.62	3.75
0.12	9.13	6.04

The measured aspect ratio ranges between 1.5 and 1.75 for all the samples, excluding the sample at $R = 0.52$ that corresponds to almost spherical particles with an average diameter as small as 3.3 ± 0.43 nm. Analogous trends in ZnO nanoparticle sizes were measured for samples grown in other alkylamines/TBPA mixtures.

The morphology of the particles and their crystallographic structure were confirmed by TEM measurements. In the absence of TBPA, ZnO crystals grew uncontrollably far beyond the size range of quantum confinement; TEM revealed a high crystallinity, but sample morphology mainly consisted of tightly agglomerated particles, having irregular shapes and sizes. In Figure 6, the typical bright field (B.F.) images obtained for ZnO samples at different R values are reported; because of the TBPA/amine capping, nanoparticles appear rather well separated on the grid, showing no tendency to aggregate.

Nanoparticles prepared at high R values (Figure 6b) exhibit a nearly spherical shape (see the corresponding HRTEM in the inset) and a narrow size distribution. A change in morphology and size as function of R was detected at much lower R values. In fact, the single nanocrystals have an elongated shape (Figure 6a), with a low aspect ratio (see the corresponding HRTEM in the inset), in agreement with the results of the XRD data fitting. In addition, a broader size distribution can be observed.

3.4. Photoluminescence. In Figure 7, the absorption spectra and the photoluminescence (excitation and emission) spectra of two selected samples of different size, synthesized at $R = 0.22$ and $R = 0.52$, respectively, are reported.

As a general behavior, the PL emission spectra of the larger nanocrystals showed a relatively narrow UV band, ascribable

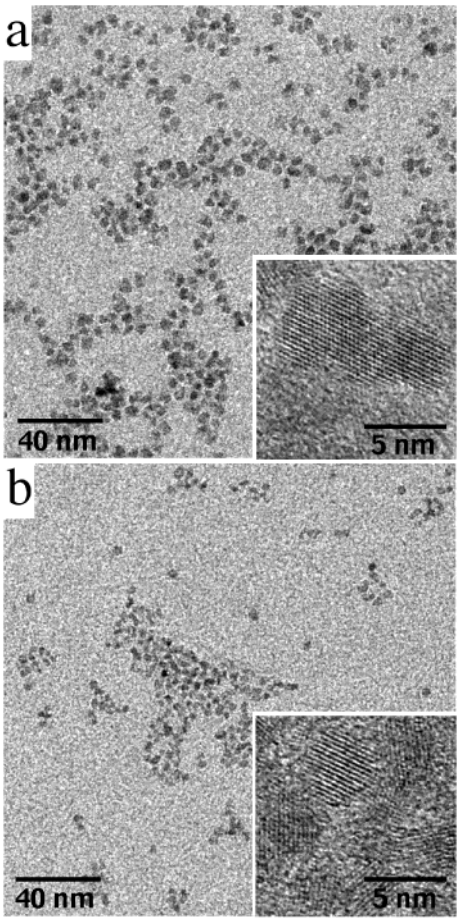

Figure 6. TEM overview of ZnO nanocrystals prepared in HDA at (a) $R = 0.12$ and (b) $R = 0.52$ by the slow heating method. In the insets (bottom right), high-resolution TEM images show highly crystalline elongated particles (a) and nearly spherical particles (b), respectively.

to band-edge recombination, and a broad intense green band. For the smaller nanocrystals, only the latter was present, blue-shifted and more intense (about 10 times) with respect to the previous case.

The position of the UV band was blue-shifted with respect to the value of the bulk ZnO band gap, with a corresponding Stokes shift from the absorption peak (~35 nm) in agreement with previously reported results.[18,32] Moreover, the red-shift of the green band from the absorption band onset increased with nanocrystal size.

In each of the two samples, the PL emission and excitation spectra show a similar behavior by changing the excitation ad the emission wavelength, respectively. In the case of smaller particles (Figure 7a, dotted line), the excitation spectrum closely resembles the corresponding absorption spectrum. The excitation spectrum of larger particles (Figure 7b, dotted line) exhibits a better-resolved exciton feature than in the corresponding absorption spectrum.

4. Discussion

In this work, the thermal decomposition of the single zinc- and oxygen-source precursor, zinc acetate, was employed to prepare acetate-free ZnO nanocrystals under inert atmosphere.[26] Amines were selected as reaction media because of their intermediate coordination strength toward Zn, when compared with surfactants such as TOPO.[29] We emphasize that zinc acetate and alkylamines do not need to be manipulated under inert

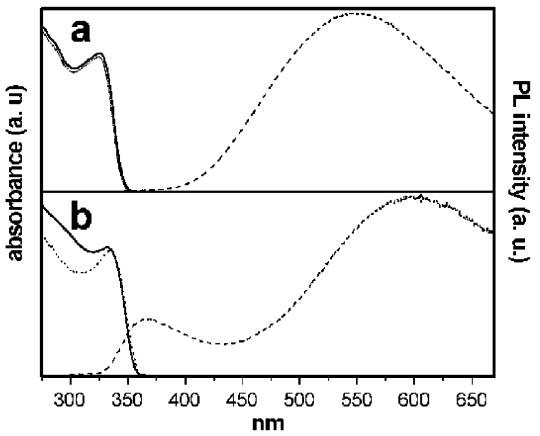

Figure 7. Normalized room temperature PL emission (dashed lines) and PL excitation (dotted lines) spectra for two ZnO selected samples grown in HDA by the slow heating method, namely, for smaller (a) at $R = 0.52$, and larger (b) at $R = 0.22$ particles. In (a**)** PL emission and excitation spectra are scaled by a factor of 10. PL emission spectra were excited at $\lambda_{ex} = 280$ nm; PL excitation spectra were recorded at $\lambda_{em} = 540$ nm (**a**) and at $\lambda_{em} = 600$ nm (b), respectively. The corresponding absorption spectra are also reported (solid line).

atmosphere, as opposed to more toxic and reactive organometallic precursors and solvents, such as alkylmetals[24] and alkyl phosphines, typically used in the high-temperature synthesis of II−VI semiconductor nanocrystals.

The results shown here demonstrate that the present route yields quantum-sized ZnO particles (3−9 nm) when TBPA is used as stabilizer. The average size of ZnO nanocrystals could be easily tuned by simply changing the TBPA/$ZnAc_2$ molar ratio in the synthesis. The possibility of achieving a controlled growth (Figure 1) allows the facile synthesis of organic-capped, nonaggregated nanocrystals (Figure 6), easily re-dispersible in organic solvents. The study of the ZnO surface by FTIR spectroscopy (Figure 4) suggested the possible presence of residual acetate groups on the nanocrystals surface; the IR spectra were dominated by the slightly shifted bands of the amine and by the strongly modified bands of TBPA, indicating an interaction between the organic coating and the nanoparticle surface. The remarkable changes observed in the P−O stretching region suggested a strong coordination of the phoshonate headgroup to the surface of ZnO, although a conclusive interpretation of the surface binding sites was difficult.

TBPA played several roles during the synthesis of ZnO nanoparticles. Long-chain alkylamines alone were ineffective in regulating the size of the particles toward a nanoscopic regime and mainly provided agglomerated (or polycrystalline) bulk ZnO. In addition, a pronounced excitonic structure (Figure 2a) is seen in the absorption spectrum, as expected for a highly crystalline material.

On the other hand, the TBPA/$ZnAc_2$ molar ratio regulates the growth kinetics of ZnO nanocrystals. We can speculate that TBPA coordinates to $ZnAc_2$ or to some decomposition intermediates, more strongly than amines, thus affecting the early stages of the synthesis. This somehow would promote a discrete nucleation event. An increase of the TBPA/precursor molar ratio resulted in a longer induction period before the appearance of ZnO features and required higher temperatures for particle formation. A hypothesis could be that nucleation and growth are governed by the decomposition of both TBPA−$ZnAc_2$ complex and "free" precursor molecules, being in equilibrium. The evidence that there are no significant differences between the direct injection and the slow heating method (Figure 3),

indicates that the nucleation and the growth stages are rather well separated in time; in the presence of TBPA, the growth rate of ZnO nanoparticles is significantly slower than the rate of the precursor decomposition. TBPA acts also as a terminating agent by coordinating the surface of the nanoparticles. In the three-stage growth regime observed in all our synthesis (induction period, fast growth, and considerably slower growth rate), a higher concentration of TBPA led to a final nanocrystal size that was progressively smaller. The combined modulation of TBPA and the reproducible growth regime provides a unique tool for designing the synthesis of ZnO crystals of a desired size in the nanoscopic regime.

The ability to control the ZnO growth can be related to the nature of complexation of Zn atoms (both in the precursor molecule and on the particle surface) during the particle growth. In our synthesis conditions, stabilizers different from TBPA probably bind too strongly to Zn atoms. In the case of TOPO, our results were in agreement with literature data, which report the formation of very stable Zn−TOPO complexes, probably inhibiting nucleation and/or growth of Zn chalcogenide nanoparticles.[29−30]

The peculiar role of TBPA could be related to the presence of the bulky *tert*-butyl end groups. In contrast to linear chains, these groups would protect a number of surface sites from being coordinated by ligand molecules. This could explain why the particles grew without dissolving in the presence of TBPA (at least for $R < \sim 0.70$), as opposed to the growth in the presence of long linear chain phosphonic acids (OPA, TDPA, and ODPA).

At present a possible role of TBPA in affecting particle morphology can be only speculated. The broadening of the size distribution observed after very long reaction times in our synthesis (Figure 1e) could be ascribed to processes such as coarsening and aggregation, which are known[9,31] to occur in solution-phase synthesis of nanoparticles. If nucleation and growth are fast, coarsening and aggregation can dominate the time evolution of the particle growth,[7,9] thus modifying the particle size and shape distribution. According to this picture, random or oriented attachment of particles can be invoked to explain the observation of elongated ZnO particles (Figure 5b) rather than spherical particles at low TBPA content. It has been reported that ZnO nanorods[32] of high aspect-ratio can be easily grown, even at almost room temperature by the oriented attachment mechanism. It might be likely that also in our synthesis conditions ($T > 200$ °C), particles start fusing into dimers (and eventually into oligomers), especially at low stabilizer concentration. In addition, TBPA could also play a specific role in affecting ZnO morphology, as surfactants[11] and polimers[14,15] can significantly influence both ZnO nanoparticle size-distribution and morphology.

The competition of radiative and nonradiative recombination mechanisms, involving surface-related defects, establishes the possibility for ZnO nanoparticles to be used as an optically active medium in light-emitting diodes. In our samples, the UV-emission (due to band-edge recombination) was observable only for nanocrystals of larger sizes (Figure 7b), with a corresponding Stokes shift from the absorption peak ascribable to electron−phonon scattering or surface shallow traps.[15,33] The dominance of the UV emission in PL spectra has been rarely observed for ZnO nanocrystals, except when their surface has been passivated by organic molecules,[13,15,33,34] or when particles from alcoholic solutions have been UV-irradiated in airless conditions.[1,35] The partial passivation of ZnO surface by TBPA/amine capping in our larger samples can be responsible for the detected band-edge luminescence.

During the past years, oxygen vacancies have been proposed to be the most likely candidates for the recombination centers involved in the visible luminescence of ZnO. It has been recently assumed that for both macrocrystalline and nanosized ZnO, the visible luminescence is due to a recombination[17,36] of a photogenerated electron from the conduction band edge (or from a shallow level close to the conduction band edge) to a deeply trapped hole in the bulk. This explanation for the visible emission agrees with our measurements, also in consideration that our nanocrystals, grown in anhydrous and oxygen-free solvents, can reasonably be oxygen-deficient.[24]

Because of the large surface-to-volume ratio in very small ZnO particles, oxygen vacancies should be mainly located on the surface, as in some cases the green emission can be even quenched by an appropriate surface capping.[15,34] Recently, the relevant role of surface in the trap emission process has been proposed[17] by invoking an efficient surface hole trapping at an O^{2-} site. In our data (Figure 7), the strong size-dependence of the overall emission intensities and of the ratio between the UV and the green band can also be explained by such a model.

By varying the detection conditions in PL excitation spectra, residual inhomogeneities were evident for samples of ZnO nanocrystals grown at low *R*. In the smaller nanocrystals sample (Figure 7a, dotted line), the accordance between absorption and PL excitation spectra demonstrated that emission was due to the same recombination process in a nearly monodisperse sample (see also Figure 6a). For the larger nanocrystal sample (Figure 7b, dotted line), PL results can be explained by invoking different or preferential emission properties[34] within an ensemble of nanoparticles, because of the presence of particle families, slightly differing in mean sizes and in the surface status. In this sample, luminescence originates from particles having a mean particle size corresponding to the exciton feature in the PL excitation spectra; smaller particles do not emit, even if they contribute to the broadening of the exciton peak in the corresponding absorption spectrum.

Hence, we reasonably assume that the emission properties of the investigated samples were related to unpassivated surface trap-states in the radiative recombination processes and that in small nanoparticles, the effect of surface dominated the PL spectra, compared to the case of large nanocrystals.

Typically, colloidal stability and luminescence intensity of ZnO nanoparticles prepared by the hydrolysis of $ZnAc_2$ depend on the amount of unidentate acetate complexes on particles surface[18] and on the excess of Zn^{2+} or OH^- ions in solution.[19] In our samples, as confirmed by IR measurements, colloidal stability could mainly be attributed to the TBPA/amine coating. Such a surface passivation undoubtedly accounted for the unchanged emission features of our samples for a few weeks after preparation at room temperature in air atmosphere.

5. Conclusions

In the present work, a novel, non-hydrolytic route to nano-ZnO of a desired size has been presented. High-quality ZnO nanocrystals (3−9 nm) were prepared by thermal decomposition of zinc acetate in amines in the presence of *tert*-butylphosphonic acid. TBPA was essential to direct particle growth to a nanoscopic regime, and the molar ratio between TBPA and $ZnAc_2$ strongly influenced both the growth kinetics and the final particle size. The various roles played by TBPA in the conditions of the synthesis have been discussed on the basis of experimental

evidence. The structural and the optical properties of such particles have been presented and comments have been made.

The above-reported synthetic scheme represents a simple, safe, and scalable approach to nanostructured ZnO and can be potentially extended to other nanoscale materials.

Acknowledgment. The authors thank Dr. A. Kornowski for TEM measurements and Dr. L. Manna for many valuable discussions.

References and Notes

(1) Spanhel, L.; Anderson, M. A. *J. Am. Chem. Soc.* **1991**, *113*, 2826−2833.

(2) Rensmo, H.; Keis, K.; Lindstrom, H.; Solbrand, A.; Hagfeldt, A.; Lindquist, S. E.; Wang, L. N.; Muhammed, M. *J. Phys. Chem. B* **1997**, *101*, 2598−2601.

(3) Bauer, C.; Boschloo, G.; Mukhtar, E.; Hagfeldt, A. *J. Phys. Chem. B* **2001**, *105*, 5585−5588.

(4) Zhang, X. T.; Liu, L. G.; Zhang, L. G.; Zhang, Y. M.; Lu, M.; Shen, Z.; Xu, W.; Zhong, G. Z.; Fan, X. W.; Kong, X. G. *J. Appl. Phys.* **2002**, *92*, 3293−3298.

(5) Johnson, J. C.; Yan, H.; Schaller, R. D.; Haber, L. H.; Saykally, R. J.; Yang, P. *J. Phys. Chem. B* **2001**, *105*, 11387−11390.

(6) (a) Marci, G.; Augugliaro, V.; Lopez-Munoz, M.; Martin, C.; Palmisano, L.; Rives, V.; Schiavello, M.; Tilley, R. J. D.; Venezia, A. M. *J. Phys. Chem B* **2001**, *105*, 1026−1032. (b) Marci, G.; Augugliaro, V.; Lopez-Munoz, M.; Martin, C.; Palmisano, L.; Rives, V.; Schiavello, M.; Tilley, R. J. D.; Venezia, A. M. *J. Phys. Chem B* **2001**, *105*, 1033−1040 and references therein.

(7) Wong, E.; Bonevich, J. E.; Searson, P. C. *J. Phys. Chem. B* **1998**, *102*, 7770−7775.

(8) Kock, U.; Fojtik, A.; Weller, H.; Henglein, A. *Chem. Phys. Lett.* **1985**, *122*, 507−510.

(9) Meulenkamp, E. A. *J. Phys. Chem. B* **1998**, *102*, 5566−5572.

(10) Carnes, C. L.; Klabunde, K. J. *Langmuir* **2000**, *16*, 3764−3772.

(11) Kaneko, D.; Shouji, H.; Kawai, T.; Kon-No, K. *Langmuir* **2000**, *16*, 4086−4089.

(12) Nyffenegger, R. M.; Craft, B.; Shaaban, M.; Gorer, S.; Erley, G.; Penner, R. M. *Chem. Mater.* **1998**, *10*, 1120−1129.

(13) Mahamuni, S.; Borgohain, K.; Bendre, B. S.; Leppert, V. J.; Risbud, S. H. *J. Appl. Phys.* **1999**, *85*, 2861−2864.

(14) (a) Taubert, A.; Palms, D.; Weiss, O.; Piccini, M.; Batchelder, D. N. *Chem. Mater.* **2002**, *14*, 2594−2601. (b) Taubert, A.; Glasser, G.; Palms, D. *Langmuir* **2002**, *18*, 4488−4494.

(15) Guo, L.; Yang, S.; Yang, C.; Yu, P.; Wang, J.; Ge, W.; Wong, K. L. *Chem. Mater.* **2000**, *12*, 2268−2274.

(16) Zou, B. S.; Volkov, V. V.; Wang, Z. L. *Chem. Mater.* **1999**, *11*, 3037−3043.

(17) Van Dijken, A.; Meulenkamp, E. A.; Vanmaekelbergh, D.; Meijerink, A. *J. Phys. Chem B* **2000**, *104*, 1715−1723.

(18) Sakohara, S.; Ishida, M.; Anderson, M. A. *J. Phys. Chem B* **1998**, *102*, 10169−10175.

(19) Monticone, S.; Tufeu, R.; Kanaev, A. V. *J. Phys. Chem. B* **1998**, *102*, 2854−2862.

(20) Che, M.; Naccache, C.; Imelik, B. *J. Catal.* **1972**, *24*, 328−335.

(21) Murray, C. B.; Norris, D. J.; Bawendi, M. G. *J. Am. Chem. Soc.* **1993**, *115*, 8706−8715.

(22) (a) Rockenberger, J.; Scher, E. C.; Alivisatos, A. P. *J. Am. Chem. Soc.* **1999**, *121*, 11595−11596. (b) Sun, S.; Zeng, H. *J. Am. Chem. Soc.* **2002**, *124*, 8204−8205. (c) Hyeon, T.; Lee, S. S.; Park, J.; Chung, Y.; Na, H. B. *J. Am. Chem. Soc.* **2001**, *123*, 12798−12801.

(23) Trentler, T. J.; Denler, T. E.; Bertone, J. F.; Agrawal, A.; Colvin, V. L. *J. Am. Chem. Soc.* **1999**, *121*, 1613−1614.

(24) Shim, M.; Guyot-Sionnest, P. *J. Am. Chem. Soc.* **2001**, *123*, 11651−11654.

(25) Wong, E. M.; Hoertz, P. G.; Liang, C. J.; Shi, B.; Meyer, G. J.; Searson, P. C. *Langmuir* **2001**, *17*, 8362−8369.

(26) (a) Audebrand, N.; Auffredic, J. P.; Louer, D. *Chem. Mater.* **1998**, *10*, 2450−2461. (b) Hiltunen, L.; Leskela, M.; Makela, M.; Niinisto, L. *Acta Chem. Scand.* **1987**, *A41*, 548−555.

(27) Hesse, M.; Meier, H.; Zeeh, B. *Spektroskopisce Methoden in der Organiscen Chemie*; George Thieme Verlag: Stuttgart, New York.

(28) (a) Gao, W.; Dickinson, L.; Grozinger, C.; Morin, F. G.; Reven, L. *Langmuir* **1996**, *12*, 6429−6435. (b) Guerrero, G.; Mutin, P. H.; Vioux, A. *Chem. Mater.* **2001**, *13*, 4367−4373.

(29) Hines, M. A.; Guyot-Sionnest, P. *J. Phys. Chem B* **1998**, *102*, 3655−3657.

(30) (a) Sigel, H.; Kapinos, L. E. *Coord. Chem. Rev.* **2000**, *200*−*202*, 563−594. (b) Clearfield, A. *Curr. Opin. Solid State Mater. Sci.* **1996**, *1*, 268−278. (c) Deluchat, V.; Bollinger, J. C.; Serpaud, B.; Caullet, C. *Talanta* **1997**, *44*, 897−907. (d) Penicaud, V.; Massiot, D.; Gelbard, G.; Odobel, F.; Bujoli, B. *J. Mol. Structure* **1998**, *470*, 31−38. (e) Deemie, R. W.; Muralidhar, R.; Knight, D. A. *J. Organomet. Chem.* **1999**, *585*, 162−166.

(31) Oskam, G.; Hu, Z.; Penn, R. L.; Pesika, N.; Searson, P. C. *Phys. Rev.* **2002**, *E66*, 114031−114034.

(32) Pacholski, C.; Kornowski, A.; Weller, H. *Angew. Chem., Int. Ed.* **2002**, *41*, 7, 1188−1191.

(33) Guo, L.; Yang, S.; Yang, C.; Yu, P.; Wang, J.; Ge, W.; Wong, G. K. L. *Appl. Phys. Lett.* **2000**, *76*, 2901−2903.

(34) Yang, C. L.; Wang, J. N.; Ge, W. K.; Guo, L.; Yang, S. H.; Shen, D. Z. *J. Appl. Phys.* **2001**, *90*, 4489−4493.

(35) Van Dijken, A.; Meulenkamp, E. A.; Vanmaekelbergh, D.; Meijerink, A. *J. Phys. Chem B* **2000**, *104*, 4355−4360.

(36) Van Dijken, A.; Janssen, A. H.; Smitsmans, M. H. P.; Vanmaekelbergh, D.; Meijerink, A. *Chem. Mater.* **1998**, *10*, 3513−3522.